Pergamon

Int. J. Heat Mass Transfer. Vol. 37, Suppl. 1, pp. 9–17, 1994

0017–9310/94 $6.00 + 0.00

0017–9310(93)E0059–P

Size effects on the temperature rise in vertical-cavity surface-emitting laser diodes

PAMELA M. NORRIS,† GANG CHEN‡ and CHANG-LIN TIEN†

†Department of Mechanical Engineering, University of California, Berkeley, CA 94720, U.S.A.;
‡Department of Mechanical Engineering and Materials Science, Duke University, Durham, NC 27708, U.S.A.

Abstract—Thin film size effects cause strong anisotropy and reduction in electrical and thermophysical material properties. This paper studies these effects and the effect of the active region radius on the temperature rise in vertical-cavity surface-emitting laser diodes (SELDs). The temperature rise in the active region of an external-cavity SELD is determined experimentally by measuring the laser output wavelength as a function of the injection current and substrate temperature. Simulation results based on models for the current flow and heat generation agree well with experimental data and they demonstrate that the thin film size effects have a strong influence on the laser temperature rise. The effect of the active region radius is clearly demonstrated by the existence of an optimal value for minimal device temperature rise.

INTRODUCTION

VERTICAL-CAVITY surface-emitting laser diodes (SELDs) have shown great application potential in optoelectronic interconnects and optical information processing [1–5]. The inherent advantages of these lasers are their low beam divergence, single longitudinal mode output, and the ease with which two-dimensional arrays can be formed and electronic devices can be integrated. These SELDs, however, have not been able to compete with conventional edge-emitting lasers despite their distinct advantages over the latter. The major reason is the strong heating that occurs when current flows across the Bragg reflectors of the laser. Heating in semiconductor lasers has numerous effects on the laser performance. It limits the gain of the active region, shifts the output wavelength, and affects the transverse mode of the laser [4–7]. As a result of the heating, the maximum continuous-wave output power from vertical-cavity SELDs has been limited to a low level.

There exist few investigations on the heating problem in SELDs. Hasnain *et al.* [5] and Tell *et al.* [7] used the laser output wavelength as a thermometer and derived the active region temperature during laser operation. Chen *et al.* [8] conducted both experimental and theoretical studies of the transient and continuous wave thermal characteristics of vertical-cavity surface-emitting lasers. Nakwaski and Osinski [9, 10] analyzed the current flow and temperature rise in etched-well SELDs using the electrical analog method. Most other simulations of the laser temperature rise employed over-simplified heat source distributions [4, 6, 11].

Vertical-cavity SELDs generally consist of an active medium embedded in two Bragg reflectors, which are multilayer structures of quarter-wavelength thin film layers. Because these layers and the active region are very thin (80–800 Å), boundary scattering of electrical carriers (electrons and holes) and heat carriers (mainly phonons) causes appreciable resistance to electrical and thermal conduction. For the current flow, it is well known that the electrical conductivity of the mirror is much lower than the corresponding bulk data of its constituting layers, owing to energy barriers formed at film interfaces [1–5]. Recent measurements [12] of the thermal diffusivity of vertical cavity SELD structures showed a strong reduction in thermophysical properties in directions both parallel and perpendicular to the superlattice plane and suggested anisotropic thermophysical properties.

This paper studies size effects, including both physical size effects of thin films and the effect of the active region radius, on the temperature rise in SELDs. Temperature rise in the active region of an external-cavity SELD is derived by measuring the laser output wavelength as a function of the injection current and substrate temperature. Modeling of the current flow and nonradiative recombination yields heat source distributions in the laser. Numerical solution of the two-dimensional axi-symmetric potential and heat con-

NOMENCLATURE

a	active region radius [m]
b	substrate radius [m]
c	specific heat [J kg^{-1} K^{-1}]
f	spontaneous emission escape factor
I	current [A]
k	thermal conductivity [W m^{-1} K^{-1}]
l	distance to cladding layer/lower mirror interface [m]
m	distance to mirror/substrate interface [m]
n	height of laser [m]
P	power [W]
q	volumetric heat generation rate [W m^{-3}]
Q	heat generation rate [W]
r	coordinate
R_e	electrical resistance [Ω]
R_t	thermal resistance [K W^{-1}]
$\mathscr{R}$	reflectance at GaAs/AlGaAs interface
T	temperature [K]
U	electrical potential [V]
V_b	junction voltage [V]
z	coordinate.

Greek symbols

α	diffusivity [s m^{-2}]
η	efficiency
ρ	density [kg m^{-3}]
σ	electrical conductivity [(Ωm)$^{-1}$].

Subscripts

eff	effective
ex	external
in	internal
o	reference
r	parallel to the substrate
sp	spontaneous emission
th	threshold
z	perpendicular to the substrate.

duction equations gives electrical potential and temperature fields inside the laser. The calculated active region temperature rise agrees well with experimental data. The results show that the reduction and anisotropy of both electrical and thermophysical properties strongly influence the thermal characteristics of the laser studied. The study also suggests an optimal active region radius for minimal temperature rise. This study can assist device-level thermal design in combination with the electrical and optical design of vertical-cavity SELDs.

EXPERIMENTAL SET-UP AND PROCEDURES

The external cavity SELD studied in this paper was grown on a p-type substrate (Zn doped 10^{19} cm^{-3}) by molecular-beam-epitaxy [2]. Figure 1(a) shows a schematic representation of the laser and Fig. 1(b) shows the coordinate system used in the analysis, as well as some reference dimensions. The p-doped (10^{19} cm^{-3}) bottom mirror consists of 33 pairs of $Al_{0.9}Ga_{0.1}As$/GaAs layers with a total thickness of 4.82 μm. The n-doped (5×10^{18} cm^{-3}) top mirror consists of seven pairs of $Al_{0.9}Ga_{0.1}As$/GaAs quarter wavelength layers with a total thickness of 1.02 μm. The interfaces between GaAs and $Al_{0.9}Ga_{0.1}As$ are digitally graded and the $Al_{0.9}Ga_{0.1}As$ layers are approximated by 9:1 (9 atomic layers to 1 atomic layer) AlAs/GaAs superlattices. The active region of the laser (designed for lasing at 980 nm) consists of three 80 Å undoped $In_{0.2}Ga_{0.8}As$ quantum wells separated by undoped 100 Å GaAs barriers, centered in an AlGaAs spacer layer of 0.3 μm thickness. This 0.3 μm thick layer, which contains the active region and the spacer, is referred to as the cladding layer. Because the top mirror has only seven pairs, it does not have a high reflectivity as in conventional SELDs. An external mirror (not shown) is employed to

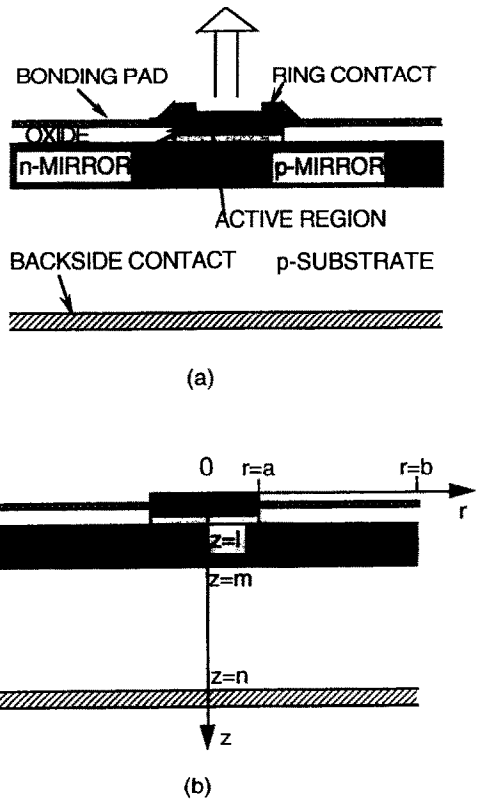

FIG. 1. (a) Schematic diagram of the laser, and (b) the coordinate system.

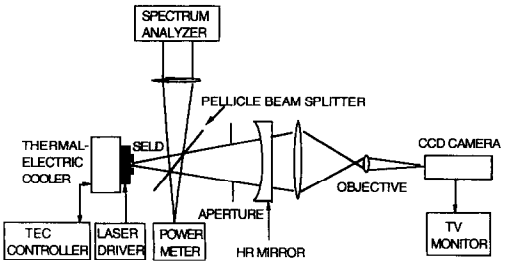

FIG. 2. Schematic diagram of the experimental set-up.

enhance the feedback to the active region. This external-cavity increases the loss of high order modes and thus enables the laser to operate at high power with a single transverse mode [2]. Also shown in Fig. 1(a) is the SiO_2 insulating layer which surrounds the active region and hence acts to confine the current. The ring contact and bonding pad are both primarily gold and are used to make the electrical connection between the laser and the external current source.

Figure 2 shows a schematic diagram of the experimental system. The laser is mounted on a thermoelectric cooler. The laser and the mirror form an external cavity. A Pellicle beam splitter sends the laser output to a spectrum analyzer, which measures the wavelength of the laser output, and to a power meter. The lasing mode is monitored by a CCD camera and a TV monitor.

The active region temperature rise during laser operation is obtained by measuring the laser wavelength as a function of the current input and as a function of the substrate temperature [5]. Heat generation in the laser raises the temperature in the active region as well as the mirror. The temperature rise red shifts the laser output wavelength because it changes the reflectance of the mirrors composing the Fabry–Perot laser cavity [5, 13]. Determination of the active region temperature consists of two steps. First, the wavelength of the laser output is measured at a fixed low current injection level while the substrate temperature is systematically varied. In this case, there is no strong heating inside the laser and the temperature rise due to current injection is negligible. Thus, the substrate temperature equals the active region temperature. Results of this measurement provide a calibration point for determining the temperature rise during laser operation. In the second step the laser output wavelength change is recorded while the injection current is systematically varied. The active region temperature is then obtained after calibration.

MODELS AND MATHEMATICAL FORMULATION

Modeling of the temperature rise in the laser consists of locating the heat source and computing the heat generation rate and temperature rise.

Heat source distributions

The major heat sources responsible for the temperature rise in external-cavity SELDs include resistive heating when current passes through the p-type Bragg reflectors, nonradiative recombination of electrons and holes, and absorption of spontaneous emission in the active region [8]. Heating in the n-type mirror can be neglected because electrons experience a much smaller resistance in the n-type mirror and also because the bonding pad facilitates lateral current flow in the n-type mirror [2, 8]. Finding the heat generation rate in the p-type superlattice requires calculating the electrical potential field and current field. In the cylindrical coordinate system shown in Fig. 1(b), Poisson's equation for the potential field in the substrate and the p-type mirror can be written as

$$\sigma_z \frac{\partial^2 U}{\partial z^2} + \sigma_r \frac{1}{r}\frac{\partial}{\partial r}\left(r\frac{\partial U}{\partial r}\right) = 0. \tag{1}$$

The boundary conditions for equation (1) are

$$z = n, \quad 0 \leqslant r \leqslant b: \quad U = 0 \tag{2}$$

$$z = 1, \quad 0 \leqslant r \leqslant a: \quad U = -U_0;$$

$$a < r \leqslant b: \quad \partial U/\partial z = 0 \tag{3}$$

$$r = 0, \quad 1 \leqslant z \leqslant n: \quad \partial U/\partial r = 0 \tag{4}$$

$$r = b, \quad 1 \leqslant z \leqslant n: \quad \partial U/\partial r = 0. \tag{5}$$

Equation (2) is the equipotential condition for the backside contact. The first half of equation (3) is the equipotential condition for the interface between the cladding layer and the lower superlattice mirror, and the second half is due to the requirement that no current flows into the insulating SiO_2 layer. Equation (4) is the symmetry requirement and equation (5) is due to the fact no current flows outside the edge of the substrate. At the substrate/mirror interface the continuity of electrical potential and current gives

$$z = m, \quad 0 < r < b: \quad U(m-0, r) = U(m+0, r) \tag{6}$$

$$\sigma_z \frac{\partial U}{\partial z}\bigg|_{z=m-0} = \sigma_z \frac{\partial U}{\partial z}\bigg|_{z=m+0}. \tag{7}$$

Solution of this potential field yields the total current at the voltage drop $(-U_0)$,

$$I = 2\pi \int_0^b \sigma_z \frac{\partial U}{\partial z}\bigg|_{z=n} r \, \mathrm{d}r \tag{8}$$

and the total electrical resistance of the lower mirror and substrate,

$$R_e = U_0/I. \tag{9}$$

The local heat generation rate due to resistive heating in the p-type mirror and the substrate is

$$q = \sigma_z\left(\frac{\partial U}{\partial z}\right)^2 + \sigma_r\left(\frac{\partial U}{\partial r}\right)^2. \tag{10}$$

When electrons and holes are injected into the active region they recombine and release energy. There are two possible recombination processes. One is radiative recombination, during which photons are generated. The other is non-radiative recombination, during which phonons (heat) are released. In addition to heat generation due to nonradiative recombination, the absorption of photons, including those emitted during spontaneous and stimulated emission processes, also generates heat. The heat generation rate in the active region can be expressed as [8, 14]

$$Q = V_b I(1 - f\eta_{sp}) \quad \text{for} \quad I < I_{th} \quad (11)$$

$$Q = V_b(I - I_{th})(\eta_{in} - \eta_{ex}) + V_b I_{th}(1 - f\eta_{sp}) + V_b(I - I_{th})\eta'(1 - f\eta_{sp}) \quad \text{for} \quad I \geqslant I_{th}, \quad (12)$$

where f is the fraction of spontaneous emission escaping the active region, I the injection current, I_{th} the threshold current, V_b the junction voltage, η_{sp} the spontaneous emission efficiency, η_{in} the internal quantum efficiency, η_{ex} the external quantum efficiency, and $\eta' = (1 - \eta_{in})$. Equation (11) is due to nonradiative recombination and absorption of the spontaneous emission. The first term in equation (12) includes loss of optical energy inside the cavity due to free carrier absorption and diffraction, the second term represents nonradiative recombination and absorption of spontaneous emission below the threshold, and the third term represents nonradiative recombination and absorption of spontaneous emission above the threshold. Chen *et al.* [8] presented an explicit formula for calculating the spontaneous emission escape factor for vertical-cavity SELD structures,

$$f = 1 - \frac{2\sin^{-1}(\mathscr{R})}{\pi}, \quad (13)$$

where $\mathscr{R}$ is the reflectance at the interface of GaAs/AlGaAs.

This work assumes that active region heating is uniformly distributed in the cladding layer. Heat source non-uniformity in the perpendicular direction does not have a significant effect because the cladding layer is only 0.3 μm thick. The large aspect ratio of the active region radius (30 μm) to the cladding layer thickness implies that edge effects can be neglected if carrier distribution along the radial direction is uniform. Computational results will show that the current injection is non-uniform, with the highest carrier intensity occurring at the edge of the active region. In this case, the outer region has a higher heat generation rate. This non-uniformity, however, does not significantly affect the temperature distribution because the inner region cannot dissipate heat effectively. This will become clear in the following discussion of local heat flux and temperature distribution.

Temperature rise in the laser

After determining the heat source distribution in the SELD, the next task is to evaluate the temperature rise. Heat conduction in semiconductor lasers is in the microscale regime because the phonon mean-free-path and wavelength become comparable to the characteristic device dimension [15]. Strictly speaking, the classical Fourier heat conduction equation is no longer valid due to interface and boundary scattering. Two different approaches exist for heat conduction in the microscale regimes. With the first approach, analysis begins from the Boltzmann transport equation. With the second approach, the Fourier heat conduction equation is used, but with a modified thermal conductivity. Because the first approach requires detailed information about the phonon scattering rate, which is not available, the present work takes the second approach. The two-dimensional axi-symmetric heat conduction equation in the coordinate system shown in Fig. 1(b) is:

$$k_z \frac{\partial^2 T}{\partial z^2} + k_r \frac{1}{r}\frac{\partial}{\partial r}\left(r\frac{\partial T}{\partial r}\right) + q = 0. \quad (14)$$

The boundary conditions for equation (14) are constant temperature at the backside contact and adiabatic boundaries for all other external surfaces. The assumption of adiabatic boundaries is reasonable because calculations on similar structures indicate that heat loss due to natural convection and thermal radiation from the top surfaces is very small compared to heat conduction into the substrate [16]. At the interfaces between different materials, the continuity of temperature and heat flux is applied.

Equation (14) neglects the temperature dependence of thermal conductivity primarily because no experimental data are available for the mirror structure. Also, the temperature dependence of the threshold current and the differential quantum efficiency are neglected in the simulation. Nakwaski and Osinski [9] considered the effect of the temperature dependence of these factors by extrapolating GaAs properties to AlGaAs and employing an empirical relationship between threshold-current and temperature. Their results show a 15% difference in temperature rise in the considered etched-well SELDs between constant properties and temperature dependent properties.

SIZE EFFECTS ON ELECTRICAL AND THERMOPHYSICAL PROPERTIES

The electrical and thermal conductivities of the laser structure are essential for solving the above equations to obtain the electrical potential and temperature fields. As mentioned before, the laser mirrors consist of quarter-wavelength ($\sim$600–800 Å) layers of GaAs and $Al_{0.9}Ga_{0.1}As$ [2], and the $Al_{0.9}Ga_{0.1}As$ compound is approximated by a 9:1 AlAs/GaAs superlattice. The major electrical resistance occurs in the direction perpendicular to the superlattice because the band gap

energies of GaAs and AlGaAs are different. Electrons can pass through the energy barrier formed at GaAs/AlGaAs interfaces only through tunneling and thermionic emission [17, 18], both of which depend on the external applied voltage. This means that the electrical conductivity in the perpendicular direction in equation (1), σ_z, is an equivalent value that depends on the externally applied voltage.

In the direction parallel to the mirror plane, electrical conduction in the p-type mirror is determined by scattering processes. The hole mean-free-path in GaAs estimated from its mobility [19] is ~ 90 Å, which is smaller than the GaAs quarter-wavelength layer thickness but larger than the thickness of the layers constituting the AlGaAs superlattice. The film interface induced reduction of hole conductivity in the GaAs layer estimated from Fuchs' model [20] is within 10% of its bulk value. Strong scattering, however, occurs in the AlGaAs layers. For current flow in the parallel direction, the equivalent electrical conductivity is determined mainly by the GaAs quarter-wavelength layers and the AlGaAs layers can be ignored because of their large resistance which is caused by carrier scattering at the AlAs/GaAs interfaces. This simplification is further supported by the observation of hole mobility in the AlGaAs compound, which is 3–5 times smaller than that in the GaAs [21]. Under this assumption, the equivalent electrical conductivity of the mirror in the parallel direction is

$$\sigma_r = d_{\text{eff}}\sigma_{\text{GaAs}}/(d_{\text{GaAs}}+d_{\text{AlGaAs}}) = 0.21\sigma_{\text{GaAs}}, \quad (15)$$

where d_{eff} is the effective GaAs layer thickness for hole transport in the parallel direction. This excludes the interface barrier layer thickness (~ 100 Å) [17] and the graded layer thickness (300 Å) [2]. With the electrical conductivity in the parallel direction fixed, the electrical conductivity in the perpendicular direction is determined by matching the resistance calculated from equation (9) with the value derived from the measured laser current–voltage characteristics [8].

The multilayer structure not only affects the electrical conductivity, but also greatly reduces the thermal conductivity. Heat conduction in GaAs and AlGaAs is mainly due to phonon transport. The phonon mean-free-path in GaAs at room temperature is about 200 Å [22], comparable to or larger than the superlattice thickness. In this case, phonons experience reflection and scattering when they travel across GaAs/AlGaAs interfaces, which greatly reduces the thermal conductivity of the superlattice structure when compared with the equivalent bulk value. Chen *et al.* [12] measured the thermal diffusivity of a similar vertical-cavity SELD structure and found that the thermal diffusivity of the superlattice is more than five times smaller than its corresponding bulk value and is anisotropic. Thermal conductivity in the parallel direction for the superlattice structure is obtained by multiplying together the measured thermal diffusivity and its equivalent heat capacity. In the perpendicular direction, the simple diffusivity and thermal conductivity relation $\alpha = k/(\rho c)$ cannot be applied due to the multilayer nature of the structure [12]. This paper uses an averaged value obtained from the upper and lower bound of the anisotropy in thermal diffusivity.

Equations (1), (10), (12) and (14) are solved numerically at each current injection level using the control volume method [23]. First, equation (1) is solved by assuming a trial value for the electrical conductivity of the bottom mirror in the perpendicular direction. Equations (8) and (9) yield the total resistance of the structure at the assumed electrical conductivity. This value is compared with the value derived from the current–voltage characteristic of the laser [8]. The whole process is repeated until the calculated resistance agrees with the measured one. With the numerical solution for the potential field, the heat generation due to resistive heating is evaluated from equation (10). The total heat source distribution is obtained by combining contributions from resistive heating with the active region heating given by equations (11) and (12). The accuracy of the numerical scheme is tested by simulating a concentric cylinder where an analytical solution exists. The convergence of the simulation is ensured by monitoring the iteration residual and refining the mesh. A total of 150×150 control volumes is used in the final computations. The problem is also solved using the finite element method. Both methods yield the same results, as expected. Table 1 lists parameters used in the simulation.

RESULTS AND DISCUSSIONS

Figure 3 displays the calibration of the laser wavelength as a function of the substrate temperature. It clearly demonstrates that the output wavelength increases linearly with heat-sink temperature. Two sets of experimental data are illustrated. One is for stimulated emission. In this case, the active region temperature is higher than the substrate temperature due to heating in the mirror and the active region. The slope of the wavelength change with temperature curve is 0.9 Å K^{-1}, larger than the value (0.6 Å K^{-1}) reported by Hasnain *et al.* [5]. This is possibly because the laser structure is different. The second set of experimental data is measured under the condition of spontaneous emission. The external mirror is removed and the current injection (5 mA) is kept at a minimal level determined by the sensitivity of the optical multimeter. The slope of the wavelength change with temperature curve for the spontaneous emission case is 1 Å K^{-1}.

The calculated and measured temperature rises in the active region are shown in Fig. 4. For currents less than the threshold current, the spontaneous emission calibration curve is used, while the stimulated emission calibration curve is used when $I > I_{\text{th}}$. The value of the active region temperature at the threshold current is determined from the measured laser wavelength under pulse operation [8]. A temperature jump of

Table 1. Parameters used in the simulation

Geometry		
active region radius a (μm)		30.0†
substrate radius b (mm)		3.00†
substrate thickness (μm)		400.0†
p-type mirror thickness (μm)		4.82†
silicon dioxide layer thickness (μm)		0.3†
bonding pad thickness (μm)		0.3†
n-type mirror thickness (μm)		1.02†
cladding and active region thickness (μm)		0.3†
total thickness of top mirror and cladding region (μm)		1.32†
total thickness of the laser (μm)		6.14†
Thermal conductivity (W m^{-1} K^{-1})		
mirrors and the active region	k_z	10‡
	k_r	12‡
silicon dioxide	$k_z = k_r$	1
substrate	$k_z = k_r$	45
gold contact	$k_z = k_r$	415
Electrical conductivity (W^{-1} m^{-1})		
GaAs substrate (10^{19} cm^{-3} p-doped)	$\sigma_z = \sigma_r$	9600§
p-type mirrors	σ_r	2016‖
	σ_z	7.26‖
Physical parameters		
center wavelength (nm)		980†
threshold current (mA)		31.4†
threshold voltage V_b (V)		1.265†
spontaneous emission efficiency, η_{sp}		0.90¶
stimulated emission efficiency, η_i		1.0††
external differential efficiency, η_{ex}		0.08†
radiation escape factor f		0.95‖

†Hadley *et al.* [2], ‡Chen *et al.* [12], §Blakemore [19], ‖Chen *et al.* [8], ¶Schnitzer *et al.* [24]. ††Hasnain *et al.* [5].

about 5 K is observed at the threshold current. This is because the measurement with spontaneous emission is done without the external mirror feedback. Calculations are carried out only for $I > I_{th}$ because the electrical conductivity can be determined from the current–voltage relation only above the lasing threshold [8]. The calculated temperature rises are in good agreement with the measured values, considering the uncertainty of the parameters used in the simulations. The calculated temperature rise increases almost linearly with injection current while the measured values increase slightly super-linearly. The experimentally measured temperature rise in Fig. 4, however, shows slight non-linearity with the injection current. This is possibly because the temperature dependence of the thermal conductivity and the spontaneous emission efficiency were neglected. The active region heating accounts for 9.4% and 6.9% of the total power dissipated at the threshold current and at $I = 95$ mA, respectively, but accounts for 25% and

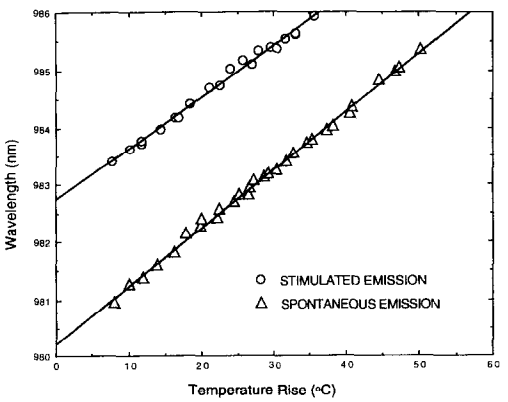

FIG. 3. Laser wavelength as a function of the substrate temperature for spontaneous and stimulated emission.

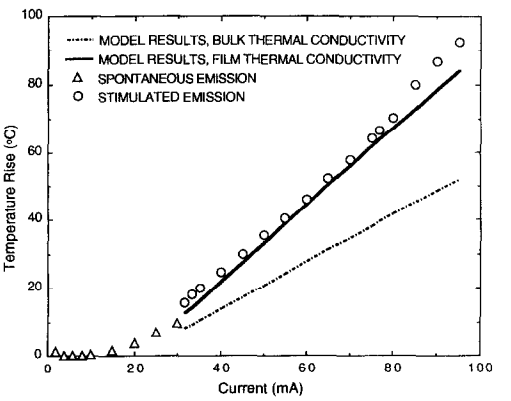

FIG. 4. Comparison of model results with experimental data.

45% of the total temperature rise at these two currents, respectively. This is because (1) heat generated in the active region has to overcome higher resistance, and (2) the current spreading in the mirror reduces the heat source intensity in this region. This point will be clear in the discussion of Figs. 5 and 6. The effects of the gold ring contact and bonding pad were also examined by removing them and repeating the analysis. Computational results indicate they do not have an appreciable effect on the total temperature rise.

The effect of reduced thermal conductivity, due to interface and boundary scattering, on the temperature rise is made clear by comparing the two different model calculations in Fig. 4. One used realistic film thermal conductivity and the other used equivalent bulk conductivity for the mirror structure. The equivalent bulk thermal conductivities used for the mirror structure are $k_z = 56\ \mathrm{W\ m^{-1}\ K^{-1}}$ and $k_r = 64\ \mathrm{W\ m^{-1}\ K^{-1}}$, calculated from the bulk thermal conductivity of GaAs and AlAs by assuming that their resistances are in series and parallel, respectively. Using bulk conductivity underestimates the temperature rises by $\sim 40\%$. This demonstrates that the thermal conductivity of the superlattice has a strong influence on the laser active region temperature even though this layer is much thinner than the substrate. The effects of electrical conductivity are also examined. The total resistance calculated from the bulk conductivity of GaAs and AlGaAs is much lower than the measured values.

A useful quantity characterizing the thermal performance of a semiconductor laser is the thermal resistance. It is defined as the ratio of device temperature rise to the power dissipated in the device,

$$R_t = \Delta T/P. \tag{16}$$

The calculated thermal resistance for the laser studied is 215 K W^{-1} at the threshold and 264 K W^{-1} at $I = 94$ mA, in reasonable agreement with the measured values of 233 K W^{-1} and 345 K W^{-1} (based on the calculated heat dissipation in the laser), respectively. Both the calculated and the measured thermal resistances are much lower than the measured values for n-type substrate SELDs ($R_t = 1788$ K W^{-1}) [5] and the calculated value for etched-well SELDs (~ 1000 K W^{-1}) [9]. There are two reasons for the lower thermal resistance of the laser studied. The first is the laser active region diameter is larger than in previous studies. The second reason is due to current spreading in the p-type superlattice. As shown in Table 1, electrical conductivity in the parallel direction in the superlattice is two orders of magnitude larger than that in the perpendicular direction. The large electrical conductivity in the parallel direction brings about a large amount of current spreading before the current funnels into the active region.

The current spreading effects can be observed from Figs. 5(a) and (b), which show the temperature rise and heat source distribution along the optical axis and

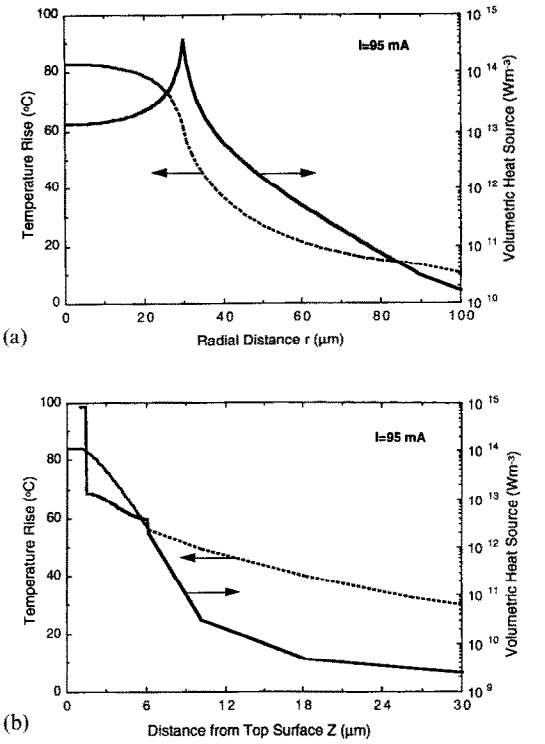

FIG. 5. Temperature and heat source distributions along (a) the interface between the cladding layer and the p-type mirror, and (b) the optical axis.

the interface between the cladding layer and the p-type mirror. When current funnels into the active region, the corner region defined by SiO_2 has the highest current density and a sharp heat source is formed there. The heat source spreads well outside the active region (to a radius of ~ 60 μm), as shown in Fig. 5(a). Figure 6 illustrates the total heat generation within a radius r as a function of the radius. At $I = 95$ mA, the total heat generated within a radius equal to the active region radius accounts for about 60% of the heat generated in the superlattice. It should be pointed out that very little heat is generated in the substrate (1.2%). Although the heat source due to resistive heating peaks at $r = a$, the temperature distribution in the

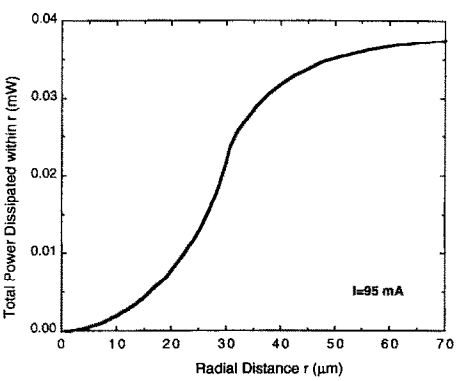

FIG. 6. Fraction of total resistive heating power dissipated within radius r.

radial direction decreases monotonically because the inner region has a large thermal resistance. From Fig. 5(b), the temperature rise in the active region and the top mirror along the optical axis is nearly uniform. This is due to the adiabatic boundary condition at the top of the laser. The temperature drop across the p-type mirror accounts for ~40% of the total temperature drop, which explains why the thermal conductivity of the superlattice structure strongly influences the temperature rise in the active region. At $I = 95$ mA, the temperature drop across the p-type mirror is 30 K. This larger temperature drop can cause an appreciable shift in the central frequency of the Bragg reflector [13] and should be taken into consideration in the design of the mirror.

An important reason for modeling the temperature rise of SELDs is to provide optimal design conditions for the improvement of laser performance. Osinski and Nakwaski [10] proposed maximizing $(I-I_{th})$ as a criterion for optimizing the laser design because the total laser power output is the same for different lasers if the external differential quantum efficiency is a constant [25]. This approach requires detailed information on the temperature dependence of the gain coefficient and the dependence of electrical conductivity on the externally applied voltage, which is often not available. Here, instead of maximizing $(I-I_{th})$, the temperature rise in the active region at fixed $(I-I_{th})$ is presented as a function of active region radius. In these calculations the threshold current density is assumed constant, which is a reasonable assumption considering that the lasing threshold is mainly determined by the carrier density [25].

Figure 7(a) shows the active region temperature rise as a function of the active region radius, with $(I-I_{th})$ and σ_z as parameters. This result can be explained by the heat generation rate due to resistive heating and the active region heating as shown in Fig. 7(b). At $I = I_{th}$, the active region temperature increases monotonically with an increasing active region radius because both the active region heating and the resistive heating increase. For $(I-I_{th}) = 30$ mA, however, the voltage drop required to drive the current into the active region is high for a small active region radius and so is the resistive heating. As the radius increases, this voltage drop decreases and the resistive heat generation reaches a minimum. Further increments in active region radius require larger currents to reach threshold and thus generate more heat in the mirror. The threshold current, and thus heat generation in the active region, always increases with radius. The net effect is the existence of an optimal radius at which the temperature rise is a minimum. Note that the minimum in resistive heating power does not coincide with the minimum in temperature, and that the increase in active region temperature after reaching the minimum point is slow compared to the rapid increase that occurs in resistive and active region heating power after the minimum point. This reflects the fact that thermal resistance due to active region heating is higher than that due to resistive heating, and that thermal resistance decreases with increasing heat transfer area. It should be pointed out that each curve in Fig. 7 is computed for a constant conductivity in the perpendicular direction, while for different radii the real conductivity is different because the voltage drop is different. A vigorous optimization of the laser radius should take into consideration the relation between voltage drop and electrical conductivity and the temperature dependence of the gain coefficient and the thermophysical properties.

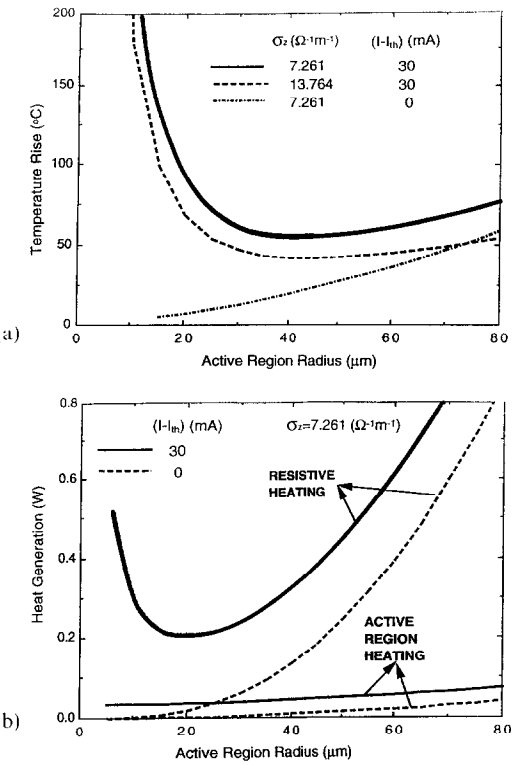

FIG. 7. (a) Temperature rise in the active region, and (b) heat generation as a function of active region radius.

Even though the laser studied has a high threshold current and relatively large threshold voltage, the above discussion demonstrates that its thermal resistance is better than other types of SELDs. With optimal mirror design and fabrication, the threshold current will be lower and the total temperature rise of the laser can be reduced.

CONCLUSIONS

Heating in surface-emitting laser diodes is the major impediment to their high power output and single mode operation. This work investigates both experimentally and theoretically the temperature rise in vertical-cavity SELDs. The temperature rise in the active region of a SELD is measured and compared with model calculations. Mathematical models are established for the current flow, heat generation, and temperature rise in the laser. The model calculations agree well with experimental results. It has been shown

that size effects on the electrical and thermophysical properties have a strong influence on the temperature rise in these lasers. The study also suggests the existence of an optimal radius for minimum active region temperature rise. These results are helpful for controlling heat dissipation and temperature rise at the device-design stage.

Acknowledgements—We would like to thank Mr M. A. Hadley and Professor J. S. Smith for providing the laser sample and their help with the experiment. P. M. Norris and C. L. Tien gratefully acknowledge the financial support of the U.S. Department of Energy and National Science Foundation. G. Chen would like to thank Dr J. Walker and Mr G. C. Wilson for useful discussions and the financial support of the Department of Mechanical Engineering and Materials Science at Duke University.

REFERENCES

1. H. Soda, K. Iga, C. Kitahara and Y. Suematsu, GaInAsP/InP surface emitting injection lasers, *Jap. J. Appl. Phys.* **18,** 2329–2330 (1979).
2. M. A. Hadley, G. C. Wilson, K. Y. Lau and J. S. Smith, High single-transverse-mode output from external-cavity surface-emitting laser diodes, *Appl. Phys. Lett.* **63,** 1607–1609 (1993).
3. J. D. Walker, D. M. Kuchta and J. S. Smith, Vertical-cavity surface-emitting laser diodes fabricated by phase-locked epitaxy, *Appl. Phys. Lett.* **59,** 2079–2081 (1991).
4. D. Vakhshoori, J. D. Wynn, G. J. Zydzik, R. E. Leibenguth, M. T. Asom, K. Kojima and R. A. Morgan, Top-surface emitting lasers with 1.9 V threshold voltage and the effect of spatial hole burning on their transverse mode operation and efficiencies, *Appl. Phys. Lett.* **62,** 1448–1450 (1993).
5. G. Hasnain, K. Tai, L. Yang, Y. H. Wang, R. J. Fisher, J. D. Wynn, B. Weir, N. K. Dutta and A. Y. Cho, Performance of gain-guided surface emitting lasers with semiconductor distributed Bragg reflectors, *IEEE J. Quan. Elec.* **27,** 1377–1385 (1991).
6. J. W. Scott, R. S. Geels, S. W. Corzine and L. A. Coldren, Modeling temperature effects and spatial hole burning to optimize vertical-cavity surface-emitting laser performance, *IEEE J. Quan. Elec.* **29,** 1295–1307 (1993).
7. B. Tell, K. F. Brown-Goebeler and R. E. Leibenguth, Thermal characteristics of deep red (0.77 μm) vertical-cavity surface-emitting lasers, *IEEE Photonics Tech. Lett.* **4,** 521–523 (1992).
8. G. Chen, M. A. Hadley and J. S. Smith, Pulsed and continuous-wave thermal characteristics of vertical-cavity surface-emitting lasers (submitted for publication).
9. W. Nakwaski and M. Osinski, Thermal properties of etched-well surface-emitting semiconductor lasers, *J. Quan. Elec.* **27,** 1391–1401 (1991).
10. M. Osinski and W. Nakwaski, Thermal properties of etched-well surface-emitting lasers and two-dimensional arrays, SPIE Vol. 1634, *Laser Diode Tech. and Appl.* **IV,** 61–83 (1992).
11. R. Baets, Considerations on geometry design of surface-emitting laser diodes, *IEE Proc.* **135,** 233–241 (1988).
12. G. Chen, C. L. Tien, X. Wu and J. S. Smith, Thermal diffusivities of GaAs/AlGaAs thin films structures, *J. Heat Transfer* (in press).
13. J. J. Dudley, D. L. Crawford and J. E. Bowers, Temperature dependence of the properties of DBR mirrors used in surface normal optoelectronic devices, *IEEE Photonics Tech. Lett.* **4,** 311–313 (1992).
14. T. Kobayashi and Y. Furukawa, Temperature distributions in the GaAs–AlGaAs double-heterostructure laser below and above the threshold current, *Jap. J. Appl. Phys.* **14,** 1981–1986 (1975).
15. C. L. Tien and G. Chen, Challenges in microscale radiative and conductive heat transfer, ASME HTD-Vol. 227, pp. 1–12 (1992).
16. G. Chen and C. L. Tien, Facet heating of quantum well lasers, *J. Appl. Phys.* **74,** 2167–2174 (1993).
17. S. Wang, *Fundamentals of Semiconductor Theory and Device Physics*, pp. 516–570. Prentice-Hall, Englewood Cliffs, NJ (1989).
18. K. Tai, L. Yang, Y. H. Wang, J. D. Wynn and A. Y. Cho, Drastic reduction of series resistance in doped semiconductor Bragg reflectors for surface-emitting lasers, *Appl. Phys. Lett.* **56,** 2496–2498 (1990).
19. J. S. Blakemore, Semiconductor and other major properties of gallium arsenide, *J. Appl. Phys.* **53,** R123–R181 (1982).
20. C. R. Tellier and A. J. Tosser, *Size Effects in Thin Films*, pp. 1–151. Elsevier, Amsterdam (1982).
21. S. Adachi (Ed.), *Properties of Aluminum Gallium Arsenide*, pp. 167–172. INSPEC, London (1993).
22. G. Chen and C. L. Tien, Thermal conductivity of quantum well structures, *J. Thermophys. Heat Transfer* **7,** 311–318 (1993).
23. S. V. Patankar, *Numerical Heat Transfer and Fluid Flow*. Hemisphere, Washington, D.C. (1980).
24. I. Schnitzer, E. Yablonovitch, C. Caneau and T. J. Gmitter, Ultrahigh spontaneous emission quantum efficiency, 99.7% internally and 72% externally, from AlGaAs/GaAs/AlGaAs double heterostructures, *Appl. Phys. Lett.* **62,** 131–133 (1993).
25. A. Yariv, *Quantum Electronics*, pp. 232–276. Wiley, New York (1989).